On the Dynamics of Equatorial Subsurface Countercurrents[1]

MICHAEL J. MCPHADEN[2]

Joint Institute for the Study of Atmospheres and Oceans, University of Washington, Seattle, WA 98195

(Manuscript received 27 December 1983, in final form 12 April 1984)

ABSTRACT

The equatorial subsurface countercurrents (SSCC) are strong, steady, geostrophically balanced eastward flows situated below the high speed core of the Equatorial Undercurrent (EUC) at ~3–5°N and S. The dynamics of these currents are explored using a continuously stratified, vertically diffusive, linear, steady state ocean model forced by zonal winds with effectively no wind stress curl. Model results agree favorably with observations in that both EUC- and SSCC-like structures are generated.

A diagnosis of the model momentum, vorticity and continuity balances at various depths and latitudes reveals that the SSCC lie outside a vertically diffusive equatorial momentum boundary layer so that both components of velocity are geostrophically balanced. They are, however, located at the poleward edge of a broader diffusive equatorial vorticity boundary layer. Within this boundary layer, cyclonic vorticity associated with the EUC diffuses to the level of the SSCC where it is balanced by poleward advection of planetary vorticity. Outside this boundary layer, the induced planetary vorticity advection is balanced by vortex stretching that weakens the temperature stratification to generate a thermostad-like structure. The SSCC are in turn geostrophically balanced by the meridional pressure gradients associated with this structure.

1. Introduction

Tsuchiya (1972, 1975) carefully documented the presence of subsurface eastward-flowing countercurrents in the eastern equatorial Pacific from geostrophic flow calculations and tracer distributions. These subsurface countercurrents (SSCC) are found in both hemispheres and are associated with isotherms plunging toward the equator at the poleward flanks of the thermostad, a thick layer of nearly homogeneous 13°C, 34.9‰ water between 150 and 300 m in the zone 5°N–5°S. The SSCC are about 150 km wide and are clearly identified with tongues of high oxygen, low nutrient and, in the Northern Hemisphere, low salinity. Their speeds and volume transports are typically 20 cm s^{-1} and 5–10 sverdrups (1 Sv = 10^6 m^3 s^{-1}). Though weaker than the Equatorial Undercurrent (EUC) and North Equatorial Countercurrent (NECC), which have transports ranging from 20 to 50 Sv, the SSCC are still significant when considering the overall mass balance of the equatorial Pacific. Flows similar to the eastern Pacific SSCC have been documented in the Atlantic (Cochrane *et al.*, 1979), but not in the Indian Ocean where seasonal monsoons dominate the wind field and where, in the mean, winds along the equator are westerly rather than easterly (McPhaden, 1982).

One can observe a distinct zonal evolution of the SSCC across the Pacific. In the central and western Pacific these currents are found progressively deeper due to the general east–west slope of the thermocline (e.g., Colin *et al.*, 1971). Moreover, while in the east they are separated from the EUC by bands of westward flow (Tsuchiya, 1981), farther to the west they are centered closer to the equator (e.g., 3°N and 3°S at 170°E; Hisard *et al.*, 1970) and are contiguous or nearly contiguous to the EUC (e.g., Fig. 1).

Tsuchiya and others (e.g., Stroup, 1969; Hayes *et al.*, 1983) have stressed that the SSCC are not simply deep extensions of the surface NECC and the weaker South Equatorial Countercurrent (SECC; Reid, 1961). The SSCC exhibit a high degree of stability in both space and time, and although there are some hemispheric differences between the northern and southern branches, they generally display remarkable symmetry about the equator. In contrast, the surface countercurrents are highly variable and asymmetric about the equator in their positions and intensity (Wyrtki, 1965, 1974) because of the highly variable and asymmetric nature of the wind stress curl (e.g., Wyrtki and Meyers, 1975), which is the essential driving force for these flows. However, while we have a conceptual framework for understanding the surface countercurrents, i.e., Sverdrup's (1947) theory, no such theoretical framework exists for explaining the SSCC. The purpose of this note is therefore to propose a simple theory to account for the flows, focusing on the central and western Pacific where they are contiguous to the EUC.

[1] JISAO Contribution No. 13.

[2] Present affiliation: School of Oceanography, University of Washington, Seattle, WA 98185.

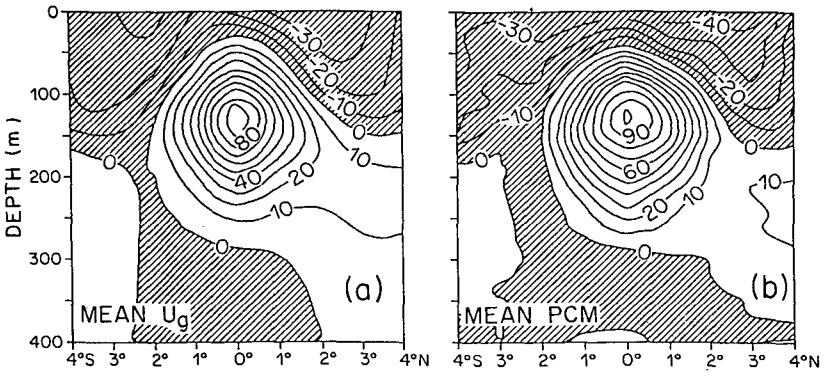

FIG. 1. (a) Meridional section of geostrophic currents (cm s^{-1}) computed from the mean pressure field of the Hawaii–Tahiti Shuttle Experiment; and (b) mean currents as measured by the PCM during the experiment. Shaded regions indicate westward flow. From Lukas and Firing (1984).

The remainder of the paper is divided into three sections. In Section 2, data from the Hawaii–Tahiti Shuttle Experiment (Wyrtki *et al.*, 1981) are discussed as they relate to the SSCC in the central Pacific. Then, in Section 3 the analytical, continuously stratified model of the steady state equatorial ocean formulated by McPhaden (1980, 1981) is reviewed, and SSCC-like featurres in this model are compared to similar features in other numerical and analytical models. Dynamical balances are then diagnosed in the vicinity of the model SSCC and compared to the Hawaii–Tahiti shuttle observations. The principal result of this study is that the SSCC are found at the poleward edge of a diffusive equatorial vorticity boundary layer driven by the meridional shear of the EUC. Finally, in Section 4 this and other results are summarized and discussed in light of the zonal evolution in flow structures in the Pacific and in view of the differences that exist between the Pacific, Atlantic and Indian Oceans.

2. The subsurface countercurrents as observed during the Hawaii–Tahiti Shuttle Experiment

The Hawaii–Tahiti Shuttle Experiment (Wyrtki *et al.*, 1981) consisted in part of 15 quasi-monthly cruises from February 1979 to June 1980. On every cruise, standard meteorological data and hydrographic data in the upper 1000 m of the water column were collected generally between 20°N and 17°S along 150, 153 and 158°W. Currents were also measured in the upper 500 m with a profiling current water (PCM) between 10°N and 6°S (Firing *et al.*, 1981). Profiles were collected at every degree of latitude and processed to a vertical resolution of 10 m. Figure 1 shows a comparison of the 15-cruise average zonal velocity as estimated from geostrophy with that measured directly by the PCM using data from all longitudes (see, Lukas and Firing, 1984). The agreement is remarkable. Both show a surface South Equatorial Current (SEC), an EUC with core speeds of ~100 cm s^{-1}, a westward Equatorial Intermediate Current (EIC; see Taft *et al.*, 1974) directly below the EUC, and SSCC below and poleward of the EUC in each hemisphere. In both sections, the northern SSCC is contiguous with the EUC, whereas there is a very weak, thin band of westward flow which separates the EUC from the southern SSCC. Standard errors for each 10 m estimate are 4 cm s^{-1} for the PCM and 20 cm s^{-1} for the geostrophic calculations.

Hawaii–Tahiti shuttle data were used to construct the temperature section in Fig. 2. In addition to a weakening of the thermocline in the vicinity of the EUC core and cold equatorial sea-surface temperatures, the figure shows a pronounced plunging of the 10–11°C isotherms near 4°N and 4°S, consistent with the geostrophic balance of the SSCC. R. Lukas (personal communication, 1983; Fig. 3) has also estimated the zonal pressure gradient between 150 and 158°W from hydrographic measurements taken during the Shuttle Experiment. He finds that relative to 900 db, the gradient near the surface is about -5×10^{-5} dyn cm^{-3}, comparable to previous estimates in this region (e.g., Knauss, 1966). In addition, he finds that the gradient reverses sign below ~150–175 m, reaching values of about $+1 \times 10^{-5}$ dyn cm^{-3}. Repeating this calculation relative to 400 db does not significantly affect the patterns or magnitudes of the zonal pressure gradients shown in Fig. 3, except to shift the zero contour downward by 10–20 m. Thus, at the level of the SSCC in Fig. 1, the zonal pressure gradient force is to the west.

Figure 4 shows that estimates of meridional velocity from the PCM are weaker and relatively much noisier than corresponding zonal velocities in Fig. 1b. Yet while any individual 10 m estimate may be highly uncertain, one can have confidence in the general pattern and magnitudes of the flow structures. In particular, off the equator in the upper 50 m there is a divergent flow with speeds of ~5 cm s^{-1}, consistent

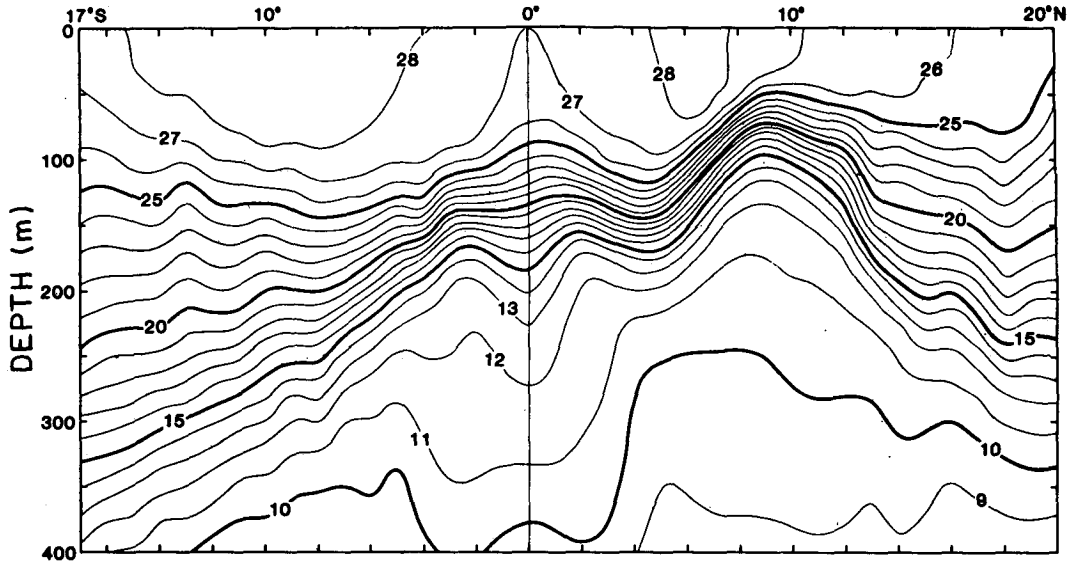

FIG. 2. Meridional section of mean temperature (°C) from the Hawaii–Tahiti Shuttle Experiment. From Wyrtki and Kilonsky (1982).

with an easterly wind stress at the surface of ~0.5 dyn cm^{-2} driving a shallow Ekman layer. Below 50 m, flow a few degrees from the equator is roughly as would be expected from a geostrophic balance. Between about 50 and 200 m, water converges on the equator at the level of the EUC with speeds of ~5 cm s^{-1}, consistent with the sign and magnitude of the pressure gradients in Fig. 3. In turn, below 200 m where the pressure gradients reverse, the meridional currents reverse and flow poleward at ~1 cm s^{-1}. These observations will be discussed further in the following section wherein a simple analytical model which produces SSCC-like structures is examined.

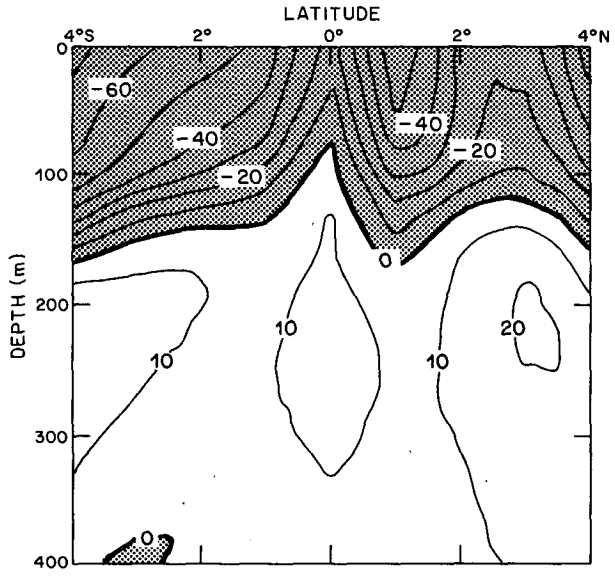

FIG. 3. Meridional section of mean dynamic height difference between 158 and 150°W relative to 900 db. Units are 100ths of a dynamic centimeter per degree longitude. (In terms of zonal pressure gradients, 50 units correspond to ~4.45 × 10^{-5} dyn cm^{-3}). Shaded portions indicate where dynamic height is higher at 158 than at 150°W, corresponding to a negative pressure gradient. From R. Lukas (personal communication, 1983).

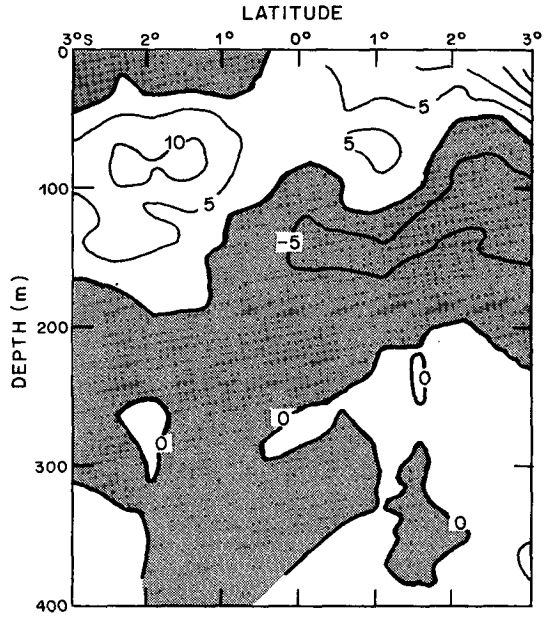

FIG. 4. Meridional section of mean meridional velocity (cm s^{-1}) as measured by the PCM during the Hawaii–Tahiti Shuttle Experiment. Shaded portions indicate southward flow. From Firing *et al.*, 1981.

3. A model of the subsurface countercurrents

a. Formulation

The model to be used for this study is briefly discussed here. A more complete description can be found in McPhaden (1980, 1981). Consider a reference atmospheric state of steady, horizontally uniform downward heat flux at the ocean surface. In an ocean with horizontally uniform thermal conductivity, this flux will generate a background vertical temperature gradient $\bar{\theta}_z$ that is a function of depth only. It is hypothesized that deviations from this atmospheric state excite perturbations (u, v, w, p, θ) around the background temperature field according to the linearized set of equations

$$-\beta y v + \rho_0^{-1} p_x = (A u_z)_z, \tag{1a}$$

$$\beta y u + \rho_0^{-1} p_y = (A v_z)_z, \tag{1b}$$

$$p_z = \rho_0 g \alpha \theta, \tag{1c}$$

$$u_x + v_y + w_z = 0, \tag{1d}$$

$$w\bar{\theta}_z = (K\theta_z)_z. \tag{1e}$$

The coordinate system is right-handed and subscripts x, y and z denote differentiation with respect to latitude, longitude and depth, respectively. We have made the standard equatorial β-plane approximation, $f = \beta y$, and the Boussinesq approximation with $\rho_0 = 1$ g cm^{-3}. The ocean is hydrostatic (1c) and density has been derived from an equation of state linearized about temperature. Eddy viscosity and heat diffusivity are A and K, respectively, and will be assumed constant, as will the background temperature gradient. Other notation in (1) is standard.

Stommel and Veronis (1957) examined (1) on the midlatitude f- and β-planes. The extension of their work to the equatorial β-plane is not straightforward because, for realistic boundary conditions, the equations will not separate in a simple way in y–z (Schneider and Lindzen, 1976). However, if one replaces the more common Laplacian diffusion in (1e) with a Newtonian cooling operator, i.e.,

$$w\bar{\theta}_z = -\frac{K}{D^2}\theta, \tag{1e'}$$

where D is a constant with units of depth, (1) can be solved by separation of variables. The equations must satisfy

$$u, v, w, p, \theta \to 0 \quad \text{as} \quad |y| \to \infty, \tag{2a}$$

with surface boundary conditions of

$$\rho_0 A u_z = \tau_0^{(x)}, \quad \rho_0 A v_z = \tau_0^{(y)},$$
$$w = 0 \quad \text{at} \quad z = 0. \tag{2b}$$

For studies of upper ocean phenomena, the bottom boundary layer can be ignored by requiring that as $z \to \infty$, all variables decay to zero.

Equations (1) and (2) can be scaled such that all terms are O(1). The equatorial trapping scale, i.e., the distance meridionally from the equator over which the most intense flows are confined, is given by

$$L = \left[\frac{A^2 N^2}{\beta^3 K}\right]^{1/5},$$

where $N^2 = g\alpha\bar{\theta}_z$ defines the Väisälä frequency. Depth, on the other hand, scales as

$$D = \left(\frac{A}{\beta L}\right)^{1/2},$$

i.e., the depth of the Ekman layer at $y = L$. Dependent variables will scale as τ_0 because of the linearity of the equations.

From (1) a single expression for v is available, solutions of which take the form

$$\left.\begin{aligned} v(x, y, z) &= \int_{-\infty}^{\infty} \sum_{n=0}^{\infty} \hat{v}_n(l, y, z) \exp(ilx)dl \\ \hat{v} &= \sum_{j=1}^{6} a_{n,j}(l)\phi_{n,j}(z)\psi_n(y) \end{aligned}\right\}, \tag{3}$$

where $a_{n,j}$ are arbitrary complex constants, l is a zonal wavenumber, ψ_n are Hermite functions and $\phi_{n,j} = \exp(m_{n,j}z)$ is the vertical dependence. The variables $m_{n,j}$ are determined by solution of the 6th-order equation which takes the form (in dimensional units)

$$\phi_{(6z)} + E_1[(2n + 1)L^{-2} + l^2]\phi_{zz} + ilE_2\phi = 0, \tag{4}$$

where

$$E_1 = \left[\frac{N^4}{AK^2\beta}\right]^{2/5} \quad \text{and} \quad E_2 = \left[\frac{\beta^3 N^8}{A^7 K^4}\right]^{1/5}.$$

Only the three roots decaying with depth are retained; two of these represent the surface trapped Ekman layers and one represents deep, quasi-geostrophic flow. There is also a solution to (1) not contained in (3), namely $v \equiv 0$, which is designated the $n = -1$ solution and which is analogous to the Kelvin wave in an inviscid ocean. Its zonal velocity component takes the form

$$u_{-1} = \sum_{j=1}^{2} a_{-1,j}\phi_{-1,j}\psi_0(y), \tag{5}$$

where $\phi_{-1,j} = \exp(m_{-1,j})$ is the solution to a fourth-order equation analogous to (4). Other fields (p, θ, etc.) can be derived from (3), (5) and (1).

McPhaden (1980, 1981) solved (1) in a zonally unbounded basin for winds of the form

$$\tau_0^{(x)} = \tau_0 \exp(il_0 x) \exp(-\gamma y^2), \quad \tau_0^{(y)} = 0. \tag{6}$$

To determine the unknown coefficients $a_{n,j}$, the series

expansion of the left side of (2b) is truncated at some $n = N_0 < \infty$ and the matrix equation

$$\mathbf{CA} = \mathbf{B} \tag{7}$$

is solved. In this expression, **A** is the vector $\{a_{n,j}\}$, **B** = $\{b_n\}$ is the vector projection of the meridional dependence of the forcing function onto Hermite functions defined by

$$\exp(-\gamma y^2) = \sum_{n=0}^{N_0} b_n \psi_n(y),$$

$$b_n = \int_{-\infty}^{\infty} \exp(-\gamma y^2)\psi_n(y)dy, \tag{8}$$

and **C** is a banded matrix of coefficients. Accurate solutions to (7) for $N_0 \gg 100$ can be found quickly and efficiently using standard techniques of linear algebra. More complex zonal structure can be introduced by superposing solutions to (7) for different l.

It should be noted that McCreary (1980) solved (1) by separation of variables in a slightly different way. He set $A = K = \nu/N^2$ and ν = constant in (1) and replaced $(K\theta_z)_z$ by $(K\theta)_{zz}$ in (1e). This allowed him to project wind forcing onto a set of vertical eigenfunctions and then to solve for the horizontal structures. Results from his model and the one discussed above compare favorably in their ability to reproduce realistic flow features for steady zonal wind forcing. Thus, in general, solutions are not very sensitive to the type of diffusion operator used in (1), as elaborated by McPhaden (1980, 1981), who also compared results for other types of diffusion operators.

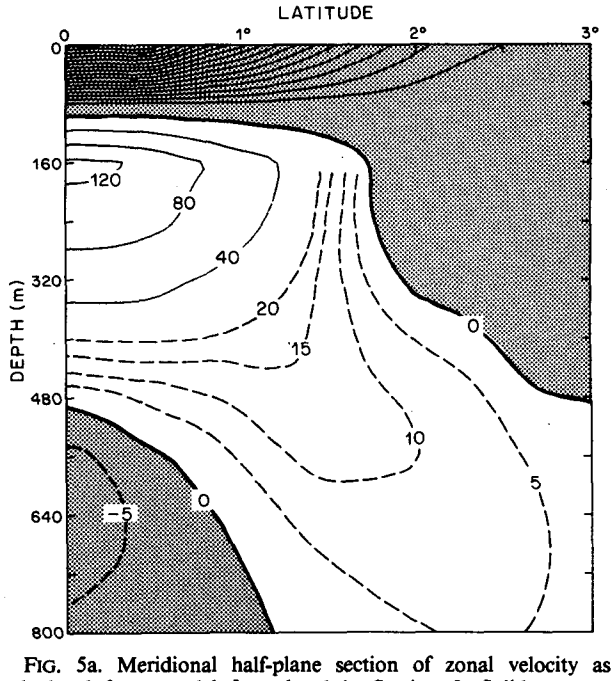

FIG. 5a. Meridional half-plane section of zonal velocity as calculated from model formulated in Section 2. Solid contour interval is 40 cm s^{-1} and dashed contour interval below the core of the EUC is 5 cm s^{-1}. Shaded regions indicate westward flow.

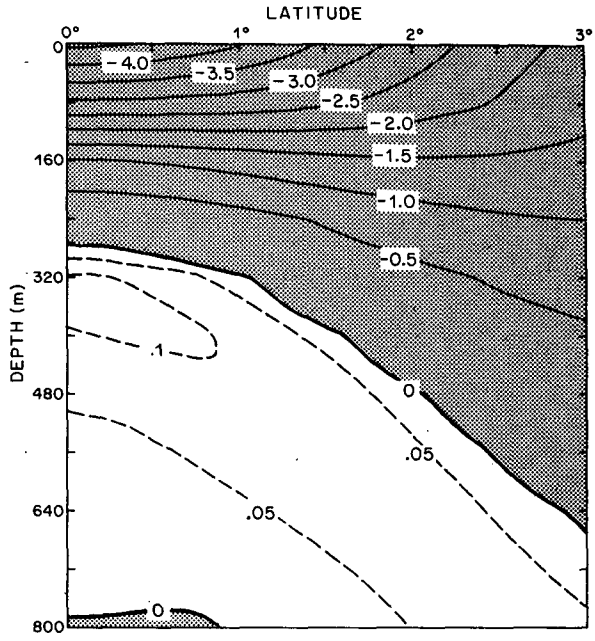

FIG. 5b. As in Fig. 5a except for zonal pressure gradient of (10^{-5} dyn cm^{-2}). Solid contour interval is 0.5 units and dashed contour interval in deeper layers is 0.025 units. Shaded regions indicate negative pressure gradients.

In the present model, A, K and N^2 are constant with depth, so that unusually intense flow develop over a distance of O(D) from the surface. The presence of these intense surface flows does not adversely affect the deeper flows, however. McPhaden (1980), for example, demonstrated that a local increase in A near the surface reduces SEC speeds without greatly modifying the model EUC. An advantage of McCreary's formulation is that it allows for specification of a mixed layer near the surface wherein $N^2 \to 0$ and $A \to \infty$ so that these otherwise unrealistically large flows are well-behaved. Thus, for the purposes of this study, the high surface speeds evident in Fig. 5 should be viewed as an inconsequential artifact of the model formulation.

In a more general sense, the fact that A, K and N^2 must be constant also means that it is impossible to generate model solutions that agree quantitatively in every detail with observations. There are significant spatial variations in these parameters which no single number can adequately characterize. Thus, when comparing the model results described below with the measurements discussed in the previous section, it is important to focus on the spatial relationships of various flow features with respect to one another rather than on, say, the absolute depth or latitude at which these features appear in the model compared with the ocean.

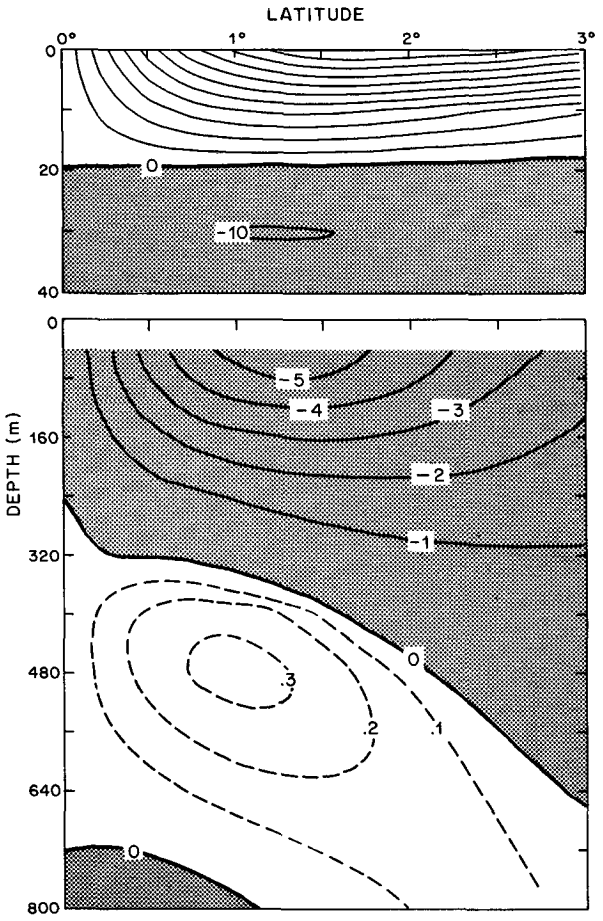

FIG. 5c. As in Fig. 5a except for meridional velocity. Solid contour interval is 10 cm s^{-1} in the upper panel, 1.0 cm s^{-1} in the lower panel; dashed contour is 0.1 cm s^{-1}. Shaded regions indicate southward flow.

The model formulation and method of solution require that the ocean be zonally unbounded. This is not a severe limitation if one is interested in modeling the open ocean steady circulation, especially in the Pacific where the basin extends over 140° of longitude along the equator. McCreary's (1980) work suggests that an imposition of meridional boundaries will only slightly affect the basic interior solution in an ocean this wide. The model must, however, be capable of generating zonal pressure gradients to drive a realistic mean circulation. In this and McCreary's (1980) model, these zonal pressure gradients are established by patterns of zonal wind stress convergence and divergence. Specification of the wind stress boundary condition for this study has been guided by observations from the Pacific which show maximum mean easterlies in the central basin with weak westerlies to the east and to the west (Wyrtki and Meyers, 1975). A similar specification was used by McPhaden (1980, 1981).

b. Results

Figure 5 shows solutions to (1) forced by winds of the form (6) with $\tau_0 = 0.5$ dyn cm^{-2}, $l_0 = 2\pi$ (20 000 km)$^{-1}$ and $\gamma^{-1/2} = 30°$ latitude. Results have been plotted at the central longitude of a 10 000 km band of easterlies where the stress is maximum. Only the Northern Hemisphere is displayed because of the symmetry of both the forcing and the response about the equator. The parameters A, K and $\bar{\theta}_z$ have been set at 5 cm^2 s^{-1}, 1 cm^2 s^{-1} and 5×10^{-4} °C cm^{-1}, respectively, such that $L = 120.8$ km and $D = 13.4$ m. Note that $L \ll \gamma^{-1/2}$ so that there is effectively no curl associated with the wind field.

Zonal velocity in Fig. 5a is similar to that shown by McPhaden (1981; his Figs. 6 and 8) except that the scales are somewhat different due to the particular combinations of parameters (A, K, $\bar{\theta}_z$, τ_0) in this study. One sees a surface SEC (too strong because of the lack of a mixed layer), an EUC centered at ~160 m with maximum speeds of ~120 cm s^{-1}, and a westward EIC of ~5 cm s^{-1} below the EUC. The most intense parts of these flows are found within a distance O(L) from the equator. In addition, there is a tongue of eastward momentum with speeds of ~10 cm s^{-1} below and poleward of the EUC, reminiscent of the SSCC in Fig. 1. This feature and its Southern Hemisphere counterpart are generated not only in this model, but also in McCreary's (1980) analytical model (his Fig. 4) and in the linear numerical calculation of Philander and Pacanowski (1980) (see Fig. 11 below).

Figure 5b shows that the zonal pressure gradient is negative (i.e., pressure is higher in the west than in the east) and of O(10^5 dyn cm^{-3}) in the SEC and upper portion of the EUC. Below the EUC core the gradient reverses and is positive. The magnitude of this reversal is weaker than observed in Fig. 3 by a factor of ~4, but otherwise the patterns and amplitudes of the model pressure gradients agree reasonably well with the observations. In particular, one sees that the pressure gradient force is westward at the depth of the model SSCC as it is in the central Pacific.

Model meridional velocities (Fig. 5c) show the same basic structures observed in Fig. 4. At the surface, there is an Ekman divergence driven by easterly winds and at the level of the EUC there is a geostrophic convergence driven by the zonal pressure gradient off the equator. In the depth range of the SSCC, there is a poleward geostrophic flow in both hemispheres consistent with the reversal of the pressure gradient, although it is somewhat smaller than observed because of the weaker model p_x.

The correspondence between the simple model and the observations invite one to diagnose the model more closely to determine the mechanisms responsible for the SSCC. To this end the momentum, vorticity

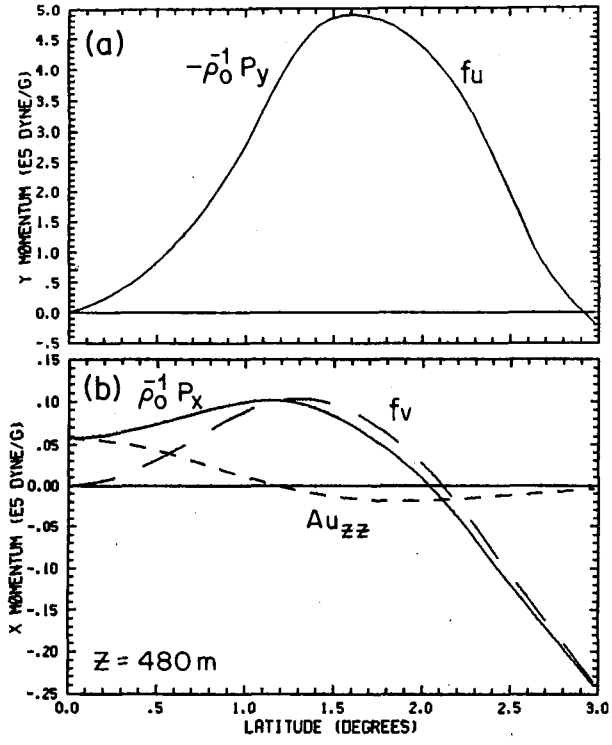

FIG. 6. (a) Balance of forces as a function of latitude in the meridional direction at a depth of 480 m as indicated in Fig. 5. Curves for fu and $-(1/\rho_0)P_y$ overlap; Av_{zz} is generally smaller by at least three orders of magnitude and therefore is not shown. (b) As in (a) but in the zonal direction.

and continuity balances have been examined as a function of latitude at several depths. Figures 6–9 show results for a depth of 480 m which is at the base of the EUC on the equator and which intersects the region of strong SSCC flow off the equator. This depth corresponds to ~250 m in Figs. 1–4.

Figure 6 shows the balance of forces in the meridional and zonal directions. The meridional balance (Fig. 6a) indicates that zonal velocity is geostrophically balanced at all latitudes, consistent with Fig. 1. The

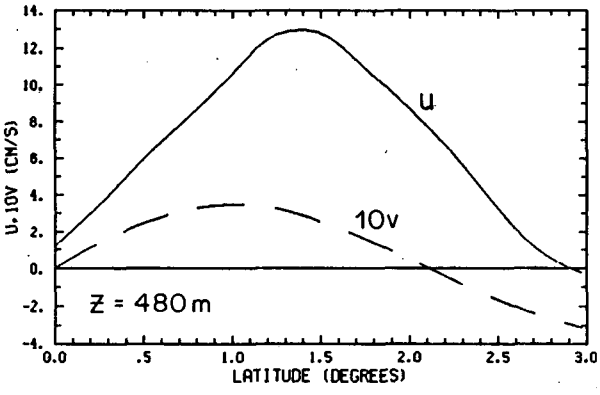

FIG. 7. Zonal and meridional velocities at a depth of 480 m.

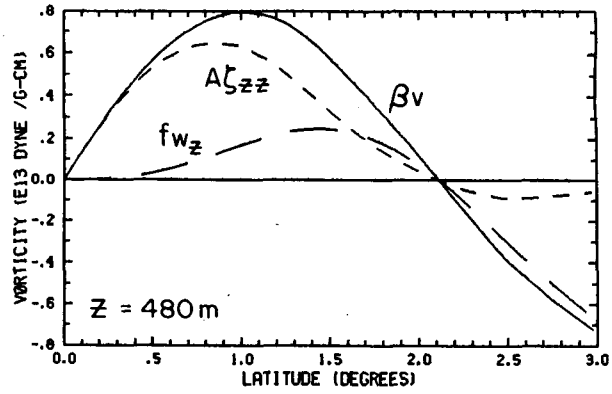

FIG. 8. Vorticity balance at a depth of 480 m.

zonal momentum balance (Fig. 6b) indicates that there is a frictional boundary layer of width $\leq 1°$ (as expected from the magnitude of L) in which the zonal pressure gradient is balanced by turbulent vertical diffusion of momentum. Outside this boundary layer, flow is geostrophic. These patterns are similar to those discussed by McPhaden (1980, 1981), where emphasis was on the EUC rather than deeper flow structures. We note, however, that the strongest flows within the SSCC lie outside the momentum boundary layer (cf. Figs. 6b and 7) so that vertical diffusion of momentum is not the mechanism responsible for these currents.

An expression for the conservation of vorticity can be derived by combining (1a), (1b) and (1d) to get

$$\beta v - f w_z = A\zeta_{zz}, \quad \zeta \equiv v_x - u_y. \tag{9}$$

The terms on the left-hand side represent advection of planetary vorticity (βv) and vortex stretching (fw_z), while the term on the right-hand side represents turbulent vertical diffusion of relative vorticity ($A\zeta_{zz}$). Figure 8 shows that within about 2° of the equator there is a diffusive vorticity boundary layer in which downward diffusion of cyclonic (i.e., positive counterclockwise) vorticity is balanced by poleward advec-

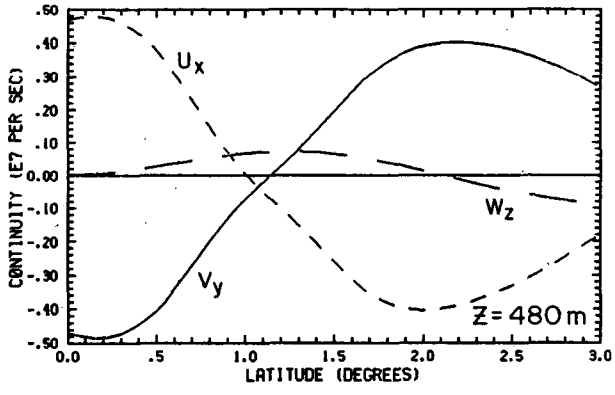

FIG. 9. Continuity balance at a depth of 480 m.

tion of planetary vorticity. The stretching term is negligible close to the equator because it is weighted by $f = \beta y \rightarrow 0$ as $y \rightarrow 0$. Outside this boundary layer, on the other hand, the balance is between the stretching and advection terms with the right side of (10) approximately zero. Figure 9 shows that the meridional divergence of mass near the equator required by these vorticity arguments is balanced by a convergence of mass in the zonal direction. Convergence/divergence in the vertical is generally weak though consistent with Fig. 8, i.e., equatorward of 2°, $w_z > 0$ and poleward of 2°, $w_z < 0$. Vertical divergence (convergence) weakens (enhances) the vertical temperature gradient so that the pattern of w_z in Fig. 9 results in a weak thermostad-like structure equatorward of 2°. While not a true thermostad in the sense that the vertical temperature gradient approaches zero, it is sufficient to generate a SSCC through the geostrophic balance (Fig. 6a).

Thus, Figs. 6–9 suggest that the model SSCC are formed when cyclonic vorticity diffuses from above, forcing poleward flow in an equatorial vorticity boundary layer. At the poleward edge of this boundary layer, the water column stretches to balance the advection of planetary vorticity, giving rise to a weak thermostad-like structure and hence geostrophic eastward flow. What is the source of this cyclonic vorticity and what sets the width of the vorticity boundary layer? These questions are answered in Fig. 10 which shows relative vorticity plotted on a meridional half-plane. (In essence, $\zeta \approx -u_y$ because $u \gg v$ and $2\pi l_0^{-1} \gg L$.) It is the meridional shear of the EUC which acts as a source of cyclonic vorticity by rotating the layers below in a counterclockwise direction. The width of the vorticity boundary layer is primarily determined by the width of this source region and is wider than that for momentum simply because the strongest shears associated with the EUC lie poleward of the strongest velocities.

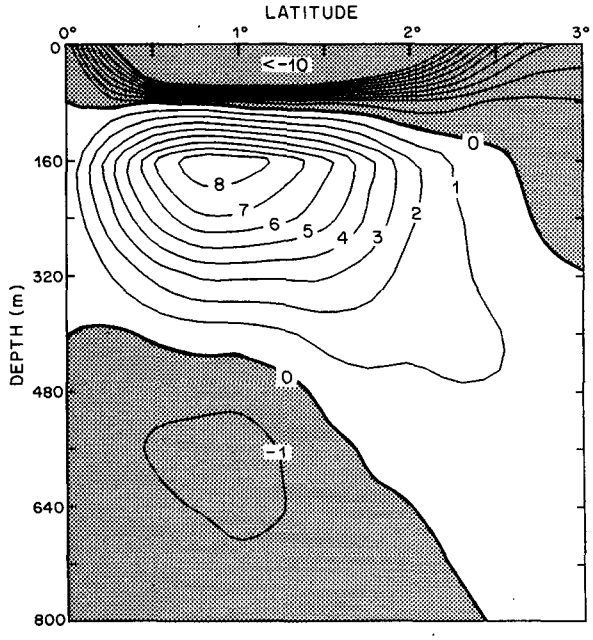

FIG. 10. As in Fig. 5 except for relative vorticity (10^{-6} s^{-1}). Shading indicates regions of anticyclonic (clockwise) relative vorticity.

In this context one can account for the slow meridional drift with depth of the SSCC axis in Fig. 5a. The SSCC, once established immediately below the EUC, has associated with it a vorticity pattern which is cyclonic on its poleward flank and anticyclonic on its equatorward flank. This shifts the source of cyclonic vorticity for the layer immediately below slightly poleward, widening the vorticity boundary layer and displacing the SSCC to a higher latitude.

4. Summary and discussion

The foregoing analysis is an attempt to understand the dynamics of the equatorial subsurface countercurrents (SSCC), strong, geostrophically balanced eastward flows below the EUC at latitudes generally between 3 and 5° in both hemispheres of the Atlantic and Pacific. These currents are found at the poleward flanks of the thermostad, a nearly homogeneous subsurface water mass found throughout much of the equatorial oceans in association with the EUC. They are, moreover, distinct from the surface countercurrents, the NECC and SECC, in that they are less variable in time and more symmetric about the equator.

Inspection of Hawaii–Tahitti Shuttle Experiment data from the central equatorial Pacific revealed several points of agreement between observed velocities and pressure gradients and those calculated from a simple analytical steady state model. The model was driven by easterlies with effectively no wind stress curl so that although an EUC and SEC were generated, no surface countercurrents appeared. The model did simulate realistic SSCC-like features, however, motivating a more careful diagnosis to determine what mechanisms were responsible for them. Results indicated that the flow at the latitudes of the SSCC is outside a diffusive equatorial momentum boundary layer and is therefore essentially in geostrophic balance. The SSCC are, however, found at the poleward edge of a diffusive vorticity boundary layer driven by the cyclonic vorticity of the EUC. This boundary layer is wider than that for momentum because within the EUC, the strongest meridional shears are located poleward of the strongest zonal current speeds. Cyclonic vorticity diffuses downward from the EUC core into the deeper ocean where it is balanced by a poleward advection of planetary vorticity. Vortex stretching becomes important at the poleward edge of the boundary layer and the resultant mass divergence spreads the thermocline to create a region of

reduced vertical temperature gradient analogous to the thermostad. The SSCC are in turn a geostrophic response to the meridional pressure gradients associated with this structure.

The above results are based on a linear calculation, so it is important to consider the possible effects that nonlinearity might have on our conclusions. Figure 11 compares linear and nonlinear numerical simulations driven by steady easterly winds (from Philander and Pacanowski, 1980). Compared to the linear results, the nonlinear EUC is narrower due to equatorward advection of eastward momentum by converging geostrophic meridional flow, and it is stretched vertically due to upwelling above the core and downwelling below (McPhaden, 1980). A narrower EUC implies an equatorward shift in the source of relative vorticity for the SSCC. However, the SSCC in the nonlinear calculation, rather than being shifted equatorward, are at approximately the same latitude as in the linear case and are separated from the EUC. This must be due to the fact that poleward flow at the depth of the SSCC tends to advect them away from the equator, counterbalancing the tendency for equatorward migration with the vorticity source of the EUC.

Strong nonlinearity could be the reason why the SSCC in the Atlantic and eastern Pacific are detached from the EUC and are found at higher latitudes than in the central and western Pacific. Near-surface eastward pressure gradient forces reverse in both oceans in the vicinity of the eastern boundary (Philander, 1973; Knauss, 1966; Lukas, 1983). A corresponding boundary enhancement of westward pressure gradient forces at the depth of the SSCC would intensify not only the poleward geostrophic flow but also the resultant displacement of the SSCC away from the equator. This effect might be felt across the width of the Atlantic because it is a relatively narrow ocean, but perhaps not felt as strongly in the central and western Pacific because of the great zonal extent of the Pacific basin.

The analytical model discussed in the previous section develops regions of reduced vertical temperature gradient but does not generate a true thermostad since nowhere in the vicinity of the SSCC does the vertical temperature gradient approach zero. This is also the case in Philander and Pacanowski's (1980) numerical model which, like the model discussed in Section 2, is formulated with constant eddy coefficients. When a Richardson-number-dependent parameterization of the eddy coefficients is incorporated into the numerical scheme (Pacanowski and Philander, 1981), a thermostad develops below the EUC core, but it is weak and narrowly confined to the equator. This casts doubt onto Jones' (1973) hypothesis that shear-generated vertical turbulent mixing is the primary cause of the thermostad. Stroup (1969) and Lukas (1983), on the other hand, suggested that the thermostad was formed in the eastern Pacific by downstream convergence of a water mass below the EUC core with thermostad temperature and salinity characteristics. Such a downstream convergence is evident below the model EUC (Fig. 9), but rather than being balanced at the equator by vertical divergence which would tend to weaken the thermal stratification there, it is balanced by a meridional divergence as required by the vorticity balance. However, the vorticity balance also requires vortex stretching at the poleward edge of a vorticity boundary layer, which should then weaken stratification away from the equator. Interestingly, in the eastern Pacific the thermostad is thickest not at the equator but rather a few degrees away (see Tsuchiya, 1975, his Fig. 1), suggesting that vortex stretching is an important mechanism in the development of the thermostad off the equator.

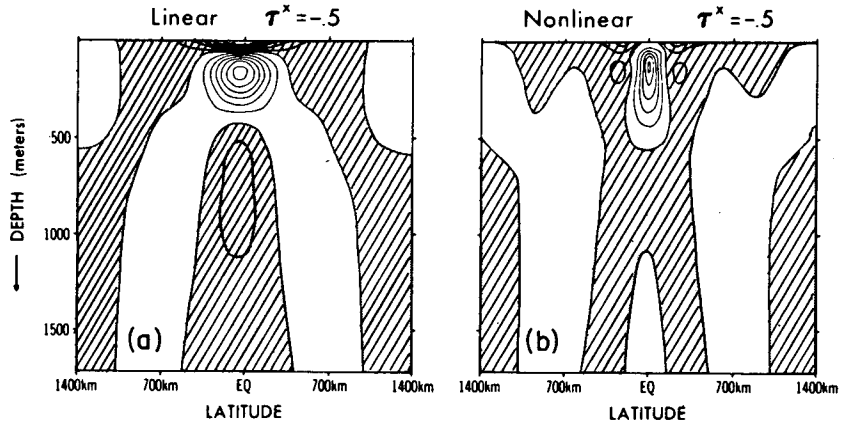

FIG. 11. A section of the zonal velocity component along the central meridian of a 5000 km wide basin (contours are at intervals of 10 cm s^{-1}). The linear case (a) is an instantaneous section at day 300. The nonlinear case (b) corresponds to averaged conditions for the period from days 300 to 350. From Philander and Pacanowski (1980).

SSCC have not been observed in the Indian Ocean where winds on seasonal time scales are dominated by monsoons and where, in the mean, winds along the equator are westerly. On the other hand, an EUC is generated in this ocean in late boreal winter and early spring under the influence of easterly winds of the northeast monsoon (e.g., Knox, 1976; McPhaden, 1982). It may be that the transient nature of this EUC does not allow sufficient time for spin-up of deeper SSCC in response to downward diffusion of relative vorticity. A frictional time scale for this spin-up would be $T_f \approx H^2/A$, where for $H \approx 100$ m and $A \approx 1$–10 cm^2 s^{-1}, $T_f \approx 10^7$–10^8 s (~4 months–3 years). This is longer than the 2–3 month lifetime of the EUC during the northeast monsoon, suggesting that steady SSCC like those found in the Atlantic and Pacific will not be generated.

Acknowledgments. The author would like to thank Dr. Hans Lass of the Institut für Meereskunde, Rostock-Wärmunde, Germany, whose interest in the subsurface countercurrents stimulated this work while he was visiting the University of Washington. Dr. Dennis Moore and Dr. Roger Lukas of the Joint Institute for Marine and Atmospheric Research (JIMAR), Honolulu, Dr. Lewis Rothstein of the University of Washington and Dr. Stanley Hayes of the Pacific Marine Environmental Laboratory, Seattle were generous with their time in discussing various aspects of this research. Dr. Lukas also kindly provided access to unpublished results of his data analysis from the Hawaii–Tahiti Shuttle Experiment and allowed the inclusion of Fig. 3 in this manuscript. This work was supported by the Joint Institute for the Study of the Atmosphere and Ocean, Seattle.

REFERENCES

Cochrane, J. D., F. J. Kelly and C. R. Olling, 1979: Subthermocline countercurrents in the western equatorial Atlantic Ocean. *J. Phys. Oceanogr.*, **9**, 724–738.

Colin, C., C. Henin, P. Hisard and C. Oudot, 1971: Le Courant de Cromwell dans le Pacifique central en février. *Cah. ORSTOM Ser. Oceanogr.*, **9**, 167–186.

Firing, E., C. Fenander and J. Miller, 1981: Profiling current meter measurements from the NORPAX Hawaii to Tahiti Shuttle Experiment. Rep. No. HIG-81-2, Hawaii Inst. Geophys., University of Hawaii, 146 pp.

Hayes, S. P., J. M. Toole and L. J. Mangum, 1983: Water-mass and transport variability at 110°W in the equatorial Pacific. *J. Phys. Oceanogr.*, **13**, 153–168.

Hisard, P., J. Merle and B. Voituriez, 1970: The Equatorial Undercurrent at 170°E in March and April, 1967. *J. Mar. Res.*, **28**, 281–303.

Jones, J. H., 1973: Vertical mixing in the Equatorial Undercurrent. *J. Phys. Oceanogr.*, **3**, 286–296.

Knauss, J. A., 1966: Further measurement of the Cromwell Current. *J. Mar. Res.*, **24**, 205–240.

Knox, R. A., 1976: On a long series of measurements of Indian Ocean equatorial currents near Addu Atoll. *Deep-Sea Res.*, **23**, 211–221.

Lukas, R., 1983: The termination of the Equatorial Undercurrent in the eastern Pacific. Submitted to *J. Mar. Res.*

——, and E. Firing, 1984: The geostrophic balance of the Pacific equatorial undercurrent. *Deep-Sea Res.*, **31**, 61–66.

McCreary, J. P., Jr., 1980: A linear stratified ocean model of the Equatorial Undercurrent. *Phil. Trans. Roy. Soc. London*, **A298**, 603–635.

McPhaden, M. J., 1980: Models of the equatorial ocean circulation. Ph.D. dissertation, University of California, San Diego, 105 pp.

——, 1981: Continuously stratified models of the steady-state equatorial ocean. *J. Phys. Oceanogr.*, **11**, 337–354.

——, 1982: Variability in the central equatorial Indian Ocean, Part I: Ocean dynamics. *J. Mar. Res.*, **40**, 157–176.

Pacanowski, R. C., and S. G. H. Philander, 1981: Parameterization of vertical mixing in numerical models of tropical oceans. *J. Phys. Oceanogr.*, **11**, 1443–1451.

Philander, S. G. H., 1973: Equatorial Undercurrent: Measurements and theories. *Rev. Geophys. Space Phys.*, **11**, 513–570.

——, and R. C. Pacanowski, 1980: The generation of equatorial currents. *J. Geophys. Res.*, **85**, 1123–1136.

Reid, J. L., Jr., 1961: On the geostrophic flow at the surface of the Pacific Ocean with respect to the 1000-decibar surface. *Tellus*, **13**, 489–496.

Schneider, E. K., and R. S. Lindzen, 1976: The influence of stable stratification on the thermally driven tropical boundary layer. *J. Atmos. Sci.*, **33**, 1301–1307.

Stommel, J., and G. Veronis, 1957: Steady convective motion in a horizontal layer of fluid heated uniformly from above and cooled non-uniformaly from below. *Tellus*, **9**, 401–407.

Stroup, E. D., 1969: The thermostad of the 13°C water in the equatorial Pacific Ocean. Ph.D. dissertation, Johns Hopkins University, 202 pp.

Sverdrup, H. U., 1947: Wind-driven currents in a baroclinic ocean; with application to the equatorial currents of the eastern Pacific. *Proc. Natl. Acad. Sci.*, **33**, 318–326.

Taft, B. A., B. M. Hickey, C. Wunsch and D. J. Baker, Jr., 1974: Equatorial Undercurrent and deeper flows in the central Pacific. *Deep-Sea Res.*, **21**, 403–430.

Tsuchiya, M., 1972: A subsurface North Equatorial Countercurrent in the eastern equatorial Pacific Ocean. *J. Geophys. Res.*, **77**, 5981–5986.

——, 1975: Subsurface countercurrents in the eastern equatorial Pacific Ocean. *J. Mar. Res.*, **33**, 145–175.

——, 1981: The origin of the Pacific equatorial 13°C water. *J. Phys. Oceanogr.*, **11**, 794–812.

Wyrtki, K., 1965: Surface currents of the eastern tropical Pacific Ocean. Bull. No. 5, Inter-American Tropical Tuna Commission, La Jolla, CA, 217–304.

——, 1974: Sea level and seasonal fluctuations of the equatorial currents in the equatorial Pacific Ocean. *J. Phys. Oceanogr.*, **4**, 91–103.

——, and G. Meyers, 1975: The trade wind field over the Pacific Ocean. Part I. The mean field and mean annual variation. Rep. HIG-75-1, Hawaii Inst. Geophys., University of Hawaii, 26 pp.

——, and B. Kilonsky, 1982: Transequatorial water structure during the Hawaii to Tahiti Shuttle Experiment. Rep. No. 82-5, Hawaii Inst. Geophys., University of Hawaii, 65 pp.

——, E. Firing, D. Halpern, R. Knox, G. J. McNally, W. C. Patzert, E. D. Stroup, B. A. Taft and R. Williams, 1981: The Hawaii to Tahiti Shuttle Experiment. *Science*, **211**, 22–28.